Materials & Design 222 (2022) 111099

Contents lists available at ScienceDirect

Materials & Design

journal homepage: www.elsevier.com/locate/matdes

Endurance testing of engineering model additive-manufactured high temperature resistojets made from Inconel 625 and tantalum

M. Robinson [a], F. Romei [a], C. Ogunlesi [a], D. Gibbon [b], A. Grubišić [a], S. Walker [a]

[a] University of Southampton, Boldrewood Campus, Burgess Road, Southampton SO16 7QF, UK
[b] Surrey Satellite Technology Ltd., Tycho House, 20 Stephenson Road, Guildford GU2 7YE, UK

HIGHLIGHTS

- An additive manufactured resistojet has been made using candidate flight materials for high temperature operation with inert or reactive propellants.
- Components additive manufactured using Inconel 625 were found to have highly repeatable behaviour during testing.
- In testing, engineering model thrusters using Inconel 625 and tantalum exceeded the required operational lifetime for small satellite propulsion applications.
- Multiphysics simulations and component-level experiments were combined to estimate the maximum temperature in the thruster.

GRAPHICAL ABSTRACT

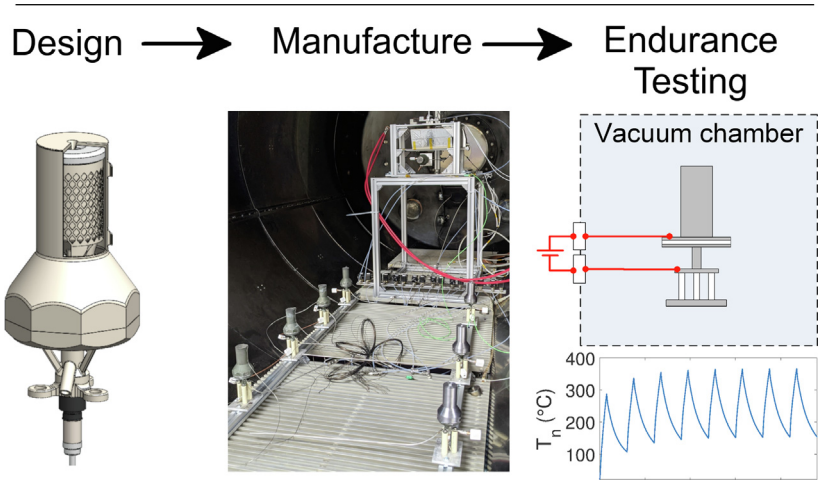

ARTICLE INFO

Article history:
Received 13 April 2022
Revised 18 August 2022
Accepted 24 August 2022
Available online 30 August 2022

Keywords:
Resistojet
Spacecraft propulsion
Additive manufacturing
All-electric spacecraft
Endurance testing

ABSTRACT

This paper reports endurance tests on engineering model high-temperature resistojets manufactured using flight-representative materials. High-temperature resistojets improve the economics of small satellites and are an attractive technology for auxiliary propulsion on all-electric geosynchronous satellites. Additive manufacturing was used to economically produce the geometrically complex heating element. Endurance tests were performed on heaters and full thruster assemblies. Eight engineering model thrusters were tested, with five manufactured from Inconel 625, and three having a tantalum heater and nozzle operating at higher temperatures. The eight units were operated in vacuum to determine their endurance. The Inconel thrusters were operated at 30 W electrical power, while the tantalum thrusters were operated at 60 W, representative of intended operating conditions. Measurements of temperature and electrical resistance throughout the tests were used to infer the condition of the thrusters. Following a retrofit of two of the Inconel 625 thrusters with a modified component to mechanically support the heater, they completed 6000 heating cycles without failure. The tantalum thrusters, equipped from the outset with the modified component, completed 10000 heating cycles. Both variants exceeded the minimum cycle requirement of 4000. This work demonstrates the operational feasibility of additive-manufactured, high-temperature resistojets.

E-mail address: m.d.robinson@soton.ac.uk (M. Robinson)

https://doi.org/10.1016/j.matdes.2022.111099
0264-1275/

1. Introduction

Propulsion systems move satellites into their operating orbits after launch, maintain the desired orbit and attitude during the mission, and remove the satellite from orbit at the end of life to prevent the creation of space debris. Two trends in the space industry have been identified which are not well addressed by currently available propulsion systems. The University of Southampton (UoS) is developing a Super-high Temperature Additive-manufactured Resistojet (STAR), which we believe to be an attractive technology option to meet the identified needs.

Satellites have become smaller, more capable, and cheaper in recent decades. The number of small satellites ($<$ 600kg) being deployed to low Earth orbit (LEO) is therefore increasing rapidly. Over 90% of all satellites launched are now in this category, numbering thousands in total [1], and this growth is expected to continue with the deployment of large constellations such as Starlink and OneWeb. The majority of these satellites will need propulsion systems, but current offerings are poorly suited for many of them. Chemical propulsion (CP) offers high thrust but is too expensive for many small companies to handle due to the extreme toxicity of hydrazine. Common plasma-based electric propulsion (EP) systems such as Hall effect (HET) and gridded ion (GIT) thrusters achieve high specific impulse (I_{sp}), but they are expensive, and moreover have low thrust-to-power ratios (TPR). Small satellites often have a tight power budget, typically 100 W or less, and the resulting low thrust necessitates long manoeuvres, reducing availability of the payload. Resistojets, a type of electrothermal propulsion, are simple, low cost, and have orders of magnitude higher TPR than plasma EP systems. However, current commercially available resistojets have very low I_{sp}. For example, the Surrey Satellite Technology Ltd (SSTL) T-30 has an I_{sp} of 48 s using xenon as propellant [2]. This limits them to very low delta-V missions. The aim of STAR is to retain the high TPR and cost effectiveness of existing resistojets, while significantly increasing I_{sp}. This would improve the economics of existing small LEO spacecraft and also be a mission-enabling technology for concepts that are restricted by the current range of available propulsion systems.

Large satellites for geosynchronous orbit (GEO) are transitioning from CP to EP to reduce propellant load. The adoption of EP for orbit raising from LEO to GEO reduced typical propellant mass ratios from over 50 % to around 10 % [3], resulting in smaller spacecraft or larger payloads, reducing costs. These benefits would be enhanced for a GEO spacecraft using only EP, enabling a single common propellant supply which would reduce dry mass and system complexity, and allow optimal use of the propellant. However, options for attitude control thrusters are limited at present. Some all-electric GEO spacecraft such as Electra [4] mount their primary electric thrusters on deployable booms, achieving the necessary pointing torque with a long lever arm rather than high thrust. This is an elegant use of the thruster, but introduces a costly, complex pointing system - besides this, Electra still uses cold gas RCS thrusters for detumbling and safe mode operations where power is limited. Resistojets have high TPR, are compatible with the xenon propellant used by the main EP thruster, and can operate in a cold gas mode. They may be used to implement an attitude control system without the use of reaction wheels or gyros [5]. However, their low I_{sp} currently outweighs all of these potential benefits. STAR, offering improved I_{sp} and high TPR in a simple, low-cost thruster, may therefore also be an enabling technology for all-electric spacecraft.

2. Background and previous work

Resistojets use a resistive electric heating element to heat a gaseous propellant, which is then accelerated from a nozzle to produce thrust. $\boldsymbol{I}_{sp}$ is proportional to the square root of the propellant's stagnation temperature T_0 as shown in Eqn. 1, where η_n is the nozzle efficiency, g_0 is the gravitational acceleration at Earth's surface, and c_p is the specific heat capacity of the propellant.

$$I_{sp} = \frac{\eta_n}{g_0}\sqrt{2 * c_p * T_0} \tag{1}$$

The SSTL T-50 operates below 900 K. The melting point of many materials far exceeds this, raising the prospect of achieving higher I_{sp}. Recently, additive manufacturing (AM) has advanced rapidly, providing a new tool to address the design and material challenges of high-temperature resistojets. AM allows highly complex components to be manufactured cheaply and quickly. High-performance aerospace nickel alloys such as Inconel 625 (In625) are already well-characterised and commonly used in selective laser melting (SLM), a particular AM technology which uses a laser to melt a bed of thin layers of metal powder. Super-high temperature refractory metals such as tantalum (Ta) can also be manufactured by SLM, though the process is not as mature as for the nickel alloys. This project aims to increase I_{sp} over current commercially available resistojets by approximately 25% using In625, and approximately 65% using Ta. Considering Eqn. 1, taking $C_p = 158$ $\mathrm{Jkg^{-1}K^{-1}}$, and assuming a realistic range for η_n of 0.9–0.95, this requires gas temperatures of 1200–1350 K for In625 or 2200–2400 K for Ta. Considering that the maximum structural temperature must be somewhat higher than the gas temperature to effect heat transfer, meeting this target may require the nickel alloy thruster's maximum temperature to be as high as 1400 K, 87% of the material's melting point. The high-temperature resistojet is designed to operate effectively below 100 W, for use on small LEO spacecraft. Separate work by the author (in a publication to follow) has experimentally confirmed that the performance target has been reached for the In625 thruster variant. Operating with xenon propellant at 3 bar supply pressure, at an input power of 32 and 58 W respectively, the thruster has an I_{sp} of 56.2$\pm$0.6 s and 61.6$\pm$0.6 s.

High-temperature resistojets were investigated as early as 1959, with NASA working to develop a thruster operating at 3000K, to achieve 1000 s $\boldsymbol{I}_{sp}$ using hydrogen propellant [6]. A concentric tubular heater design was used - a central tube was heated by an electric current, surrounded by a number of unpowered tubes, indirectly heated by radiative transfer from the central tube. Propellant flowed axially through the annular channels between the tubes, beginning in the outer channel and circulating radially inwards. The cold propellant flow in the outer channels led to high thermal efficiency by capturing heat that would otherwise be lost from the casing. The long flow path allowed propellant temperatures to approach the structural temperature, reaching the highest possible $\boldsymbol{I}_{sp}$. Experimental tests on the ground measured $\boldsymbol{I}_{sp}$ of 700 s, indicating a temperature in excess of 2200K, in the range of interest for STAR. However, the resistojet operated at 30 kW, and required complex, costly manufacturing processes: chemical vapour deposition to produce thin tungsten tubes, and electron-beam welding to fabricate the heater assembly. The research was curtailed following the introduction of plasma electric propulsion that produced higher I_{sp}, using more practical propellants.

Development of a high-temperature AM resistojet at the UoS began in 2014, with the doctoral research of Dr. Federico Romei. Romei adapted the concentric tubular resistojet concept for AM, to capture the benefits of the design with more cost-effective manufacture. He designed and manufactured a prototype thruster referred to hereafter as STAR-0. Fig. 1 shows a cutaway view of the CAD design for STAR-0, alongside a view of the propellant flow path. Through several iterations, Romei's work demonstrated the feasibility of an AM tubular resistojet concept [7], using SLM to

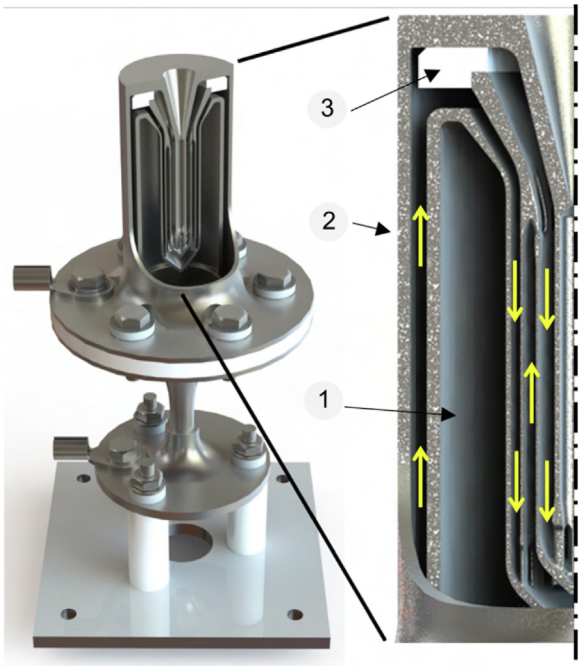

Fig. 1. Rendered CAD cutaway of STAR-0 thruster prototype mounted on thrust balance interface plate. Labelled features: 1 - AM heat exchanger/nozzle, 2 - pressure case, 3 – ceramic nozzle spacer. Yellow arrows in right-hand view show propellant flow direction. Thruster interface plate at bottom left is 58 x 58 mm and assembly height is 107 mm.

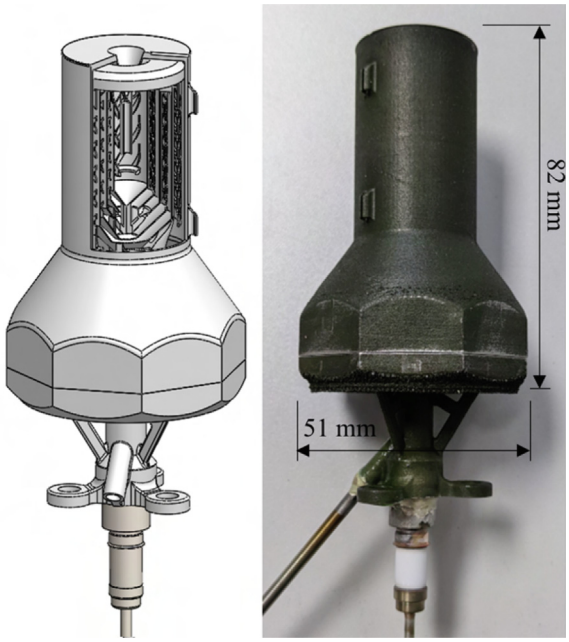

Fig. 2. Left: cutaway CAD image of BB-02 design, showing assembly arrangement of heating element within thruster. Right: photograph of thruster assembly.

produce high-aspect ratio thin-walled heater tubes in a complex configuration with an integrated supersonic nozzle. Through laboratory thrust measurements, he verified that the I_{sp} of a stainless steel 316L prototype model was comparable to that of the SSTL T-50 [8].

As part of an environmental testing campaign to raise the TRL of the STAR technology, endurance testing of two STAR-0 thrusters was carried out by the author [9]. An endurance target of 4000 cycles was chosen based on information provided by SSTL, representing an upper bound on typical applications of the thruster as the primary propulsion system of a small LEO satellite. The design was found to be susceptible to early failures induced by thermo-mechanical cycling, with the two units under test failing before reaching 10% of the endurance target. The resistojet was subsequently redesigned to extend its lifetime. The objective of the redesign was to reduce the magnitude of stresses developed by mismatched thermal expansion between the concentric tubes that make up the heating element. The new design, referred to hereafter as BB-02, is the subject of the tests described in this paper.

3. BB-02 thruster design

BB-02 was developed as an engineering model. Fig. 2 shows a CAD image of the design and a photograph of a full engineering-model thruster assembly. The concept is substantially the same as STAR-0, consisting of a series of nested annular flow channels between concentric tubes, where cold propellant is introduced at the outer radius before flowing radially inwards, passing back and forth axially. An electric current flows through the heater, and the heat thus generated is transferred to the propellant. The long flow path maximises propellant temperature, and the inward radial flow allows the initially cold propellant to capture heat which has been conducted to the exterior of the heater, improving thermal efficiency compared to a single pass. The key differences between STAR-0 and BB-02 consist of: the introduction of flexible elements into the heater to compensate for mismatched thermal expansion; the separation of the heater from the nozzle, which was printed as an integral piece in STAR-0; and changing from a permanent welded construction to the use of screws. The new design is covered by a pending patent [10].

Two variants have been manufactured using different materials. The high-temperature variant, STAR-Ta, is made from refractory metals, which offer the highest potential resistojet performance but entail high technical risk due to the low level of technological maturity of refractory metal AM. Three candidate materials were considered: tantalum, tungsten and rhenium. All have a melting point above 3000 °C. Tungsten has the highest melting point at 3422 °C, and is the cheapest. Tantalum has the lowest melting point at 3017 °C, is somewhat more expensive, but is superior to tungsten for this application as it does not embrittle upon exposure to high temperature. Rhenium has an intermediate melting point and shares the high temperature ductility of tantalum, however it is very expensive, costing thousands of pounds per kilogram. Tantalum was therefore chosen as the base material, as its melting point is still significantly higher than the planned 2400 K operating temperature. In component-level testing, both pure tantalum and a tantalum-10% tungsten alloy (which retains most of the ductility of pure tantalum while increasing the melting point) were tested. For the intermediate-temperature variant, STAR-Ni, nickel superalloys were identified as a technologically mature group of materials, widely used in high-temperature aerospace applications, which can sustain higher temperatures than the state-of-the-art resistojets. Moreover, some nickel superalloys are already widely available for manufacturing by SLM. Following an earlier test campaign, Inconel 625 was chosen.

STAR is initially envisaged to operate with xenon propellant. It has been used by SSTL for several missions with their T-30 resistojet because of its high storage density, and it is the most common propellant used by plasma EP systems, giving compatibility with all-electric spacecraft. Considering inert propellants such as xenon, STAR-Ta represents a high-risk but high-reward development, utilising the highest temperature materials. STAR-Ni represents a lower reward path with lower risk, as the materials are well known

in the aerospace industry and commonly used. However, despite the lower temperature ceiling, STAR-Ni has the benefit of being compatible with a wider range of propellants, including oxidising or reactive substances such as steam and iodine, both of which have received recent attention as alternative propellants for EP. Therefore Inconel 625 has the potential for greater flexibility in future.

4. Experimental endurance testing

Endurance testing was carried out on BB-02 to investigate the extent to which the new design improved cyclic endurance over STAR-0. Testing was carried out in two stages. First, component-level tests were performed on the heater, then tests were conducted on full engineering model (EM) thruster assemblies.

4.1. Test specimens

For component-level tests, ten Inconel 625 (In625) heaters, three tantalum (Ta) heaters and two tantalum-10% tungsten (Ta10W) heaters were tested. As part of a consortium under a UK Space Agency Flagship grant, the heaters were produced by HiEta Technologies Ltd, an industrial manufacturing partner. They were manufactured on a Renishaw AM250 SLM machine. The In625 parts were manufactured with a layer thickness of 60 μm and a laser energy density of 2.86 Jmm^{-2}. The Ta parts were manufactured with a layer thickness of 30 μm and a laser energy density of 7.14 Jmm^{-2}. As a full AM parameter development was outside the scope of this work, the Ta10W parts were manufactured using the same parameters as pure Ta. The Ta and Ta10W powder was manufactured and provided by H.C. Starck Inc. The parts were stress relieved before removal from the build plate by HiEta. The parts were visually inspected by the author, paying special attention to the coil and mesh elements of the heaters, which were the most challenging to manufacture. All heaters were ultrasonically cleaned at the University of Southampton with warm isopropanol to remove contaminants including any remaining metal powder. Parts were weighed before and after cleaning, with additional rounds of cleaning undertaken until there was no further change, indicating the removal of all loose powder. The room-temperature electrical resistance of each heater was measured before and after each cleaning step, and compared between heaters as an indicator that the coil had not been significantly damaged or deformed. The number of refractory parts was lower than the number of nickel alloy parts due to the difficulty of obtaining the necessary quantities of tantalum powder suitable for AM. For this reason, while all In625 parts under test were manufactured in a single batch, one of the Ta heaters was from a different manufacturing batch to the other two.

For assembly-level testing, five thrusters were produced with nozzles and heaters made from In625, and three had Ta heaters and nozzles. All other AM components were made from Inconel 625 in both variants, as they are not exposed to the highest temperatures in the thruster. All AM components were supplied by the same industrial partner as the component-level test specimens, and the number of Ta thrusters was again limited by material availability. Due to the low Ta powder quantities, a "reduced build volume" add-on was used in the SLM machine, whose total height was too short to build the Ta nozzles. Therefore, they were machined. The machined nozzles were made with thicker walls than the printed design to ensure manufacturability, but were otherwise identical. Post-build machining was carried out in the Engineering Design and Manufacturing Centre (EDMC) at UoS. All parts were ultrasonically cleaned with warm isopropanol to remove contaminants before assembly. Table 1 shows the material of the heater and nozzle for each assembly, and the mass and cold resistance of the heater before and after ultrasonic cleaning. The Inconel 625 heaters were highly consistent, with a relative standard deviation (RSD) in their cold resistance of 1.1% after cleaning. The Ta heaters were more variable, with an RSD of 9.1% after cleaning. The In625 heaters were clear of loose powder on receipt, with only one heater having a measurable mass difference before and after, and little powder visible in the beaker after cleaning. The Ta heaters, meanwhile, lost an average of 75 mg of powder during cleaning.

Table 1
Properties of EM thruster assembly heaters before and after ultrasonic cleaning. Brackets indicate the material used for the heater and nozzle of the assembly.

#	Mass (g)	R (mΩ)
1 (In625)	28.61, 28.61	141.0, 141.7
2 (In625)	28.41, 28.41	142.7, 143.0
3 (In625)	28.46, 28.46	141.3, 142.0
4 (In625)	28.55, 28.54	145.0, 145.7
5 (In625)	28.49, 28.48	141.1, 141.3
6 (Ta)	58.86, 58.79	17.7, 16.7
7 (Ta)	59.41, 59.27	16.3, 16.0
8 (Ta)	58.11, 58.06	19.7, 20.0

4.2. Test methodology

A common overall test methodology was followed for all experiments, with some details of implementation varying. The specimens were subjected to thermal cycling representative of planned operating conditions, by applying power to the heater as in operation. The test protocol was developed for this work based on information provided by Surrey Satellite Technology Ltd. in their role as an industrial partner. They provided representative requirements based on the flight heritage of their T-30 resistojet, a small thruster operating at 30 W and used for orbit-raising and maintenance on several small spacecraft including the RapidEye constellation, the UK Disaster Monitoring constellation, and GIOVE-A - the latter of which also used the thrusters for attitude control. SSTL's experience indicated that 4000 heating cycles would envelope typical missions in which STAR would be used in similar roles on small LEO spacecraft. In this application, a typical thrust event may last 1-5 min, limited in different cases by the desire to maximise efficiency by thrusting as close to apogee/perigee as possible, or by the need to reject torque from thrust misalignment. A cycle time of 5 min heating and 5 min cooling was therefore chosen for the component-level testing. At the time of testing the EM thruster assemblies, a cycle time of 2 min heating and 2 min cooling was chosen. The duration was reduced as a result of time constraints in the testing facility, to ensure sufficient cycles could be completed. 2 min was still considered to be a representative operating time with respect to the industrial requirements. Moreover, experience in testing of STAR heaters indicated that the centre of the heater approached its maximum temperature in less than a minute, ensuring the reduced test time remained representative from the perspective of likely failure modes.

The tests were carried out in three runs. First, all In625 heaters were tested simultaneously, then all refractory heaters, and then all In625 and Ta thruster assemblies together. Tests were performed in the vacuum facility of the David Fearn electric propulsion laboratory at the University of Southampton. The facility consists of a main chamber (2 m diameter × 4 m length) and a smaller loading chamber (0.75 m diameter × 0.7 m length) separated by a pneumatically actuated gate. The loading chamber was used for component-level testing. It is fitted with a Leybold Turbovac MAG W 700 iP turbomolecular pump backed by an Edwards XDS 35i scroll pump with a pumping rate of $40 m^3 h^{-1}$,

and a Pfeiffer Vacuum PKR 251 gauge with a combined range from 5×10^{-9} mbar to atmospheric pressure. The main chamber was used for assembly-level testing. It is fitted with two Leybold Turbovac MAG W 2200 iP turbomolecular pumps backed by an Oerlikon Leybold LV140C roughing pump, in addition to two Leybold Coolpower 140T cryopanels each powered by a Leybold Coolpack 6000H compressor, and another PKR 251 gauge. Testing was carried out at chamber background pressures not greater than 1×10^{-2} mbar.

Fig. 3 shows the generic test setup. This is described first, followed by the specific implementation for each set of tests. DC electric power was supplied to each test specimen using a Kikusui PWX1500L power supply unit (PSU) operated in constant current mode, with different currents chosen for each material based on the intended power and the specimens' resistance. To make the best use of testing time, the specimens in each test were wired up to form 2 groups. Specimens in each group were connected in series, with one end of each group permanently connected to the ground terminal of the PSU, while the other end of each group was switched alternately to the positive terminal by a pair of Schneider SSP1D440BDT solid-state relays. In this way, one group was heated while the other cooled. The voltage across the terminals of each specimen was measured by a National Instruments NI-9205 analogue input module in an NI cDAQ-1988XT CompactDAQ chassis. The current supplied to the specimens was measured using a Murata Power Solutions 3020–01096-0 shunt with 1 mΩ resistance, the voltage across which was measured by the NI-9205 module. Temperature measurements of specimens were made using type K thermocouples read out by an NI-9213 module. Thermocouple locations differed for each test due to the different operating temperatures. The positions are shown in Fig. 4 for the component level tests. Control of the PSU and relays, and collection/output of all measurements, was performed by a custom LabVIEW program.

In625 component-level tests were carried out with 10 identical heaters, connected to the PSU in 2 groups of 5. The specimens were heated for 5 min and cooled for 5 min in each cycle. The supply current was set to 14 A, chosen in a preliminary test to provide the desired heating power of 30 W at the beginning of life. The vacuum chamber had 10 thermocouple feedthroughs. Two heaters were equipped with two thermocouples, in locations 1 and 2 as shown in Fig. 4. Six more were equipped with a single thermocouple in location 2, and two had no thermocouples. This distribution was chosen to allow comparison between the bare and instrumented heaters, to ensure the presence of the thermocouples did not affect the temperature distribution given the low power of the heaters. The thermocouples used were bare junctions spot-welded directly to the heaters. Fig. 5 shows the test setup. The heaters were mounted to a test rig which replicated the mechanical and electrical interface of the thruster.

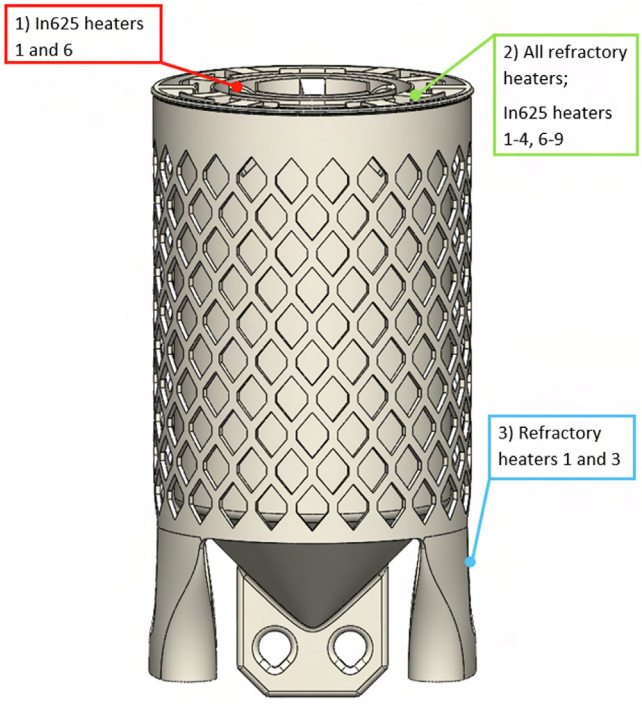

Fig. 4. Locations of thermocouple attachments on heaters for component-level life-testing.

Refractory metal component-level tests were carried out in the same way as for In625, with one group of 3 Ta heaters and one

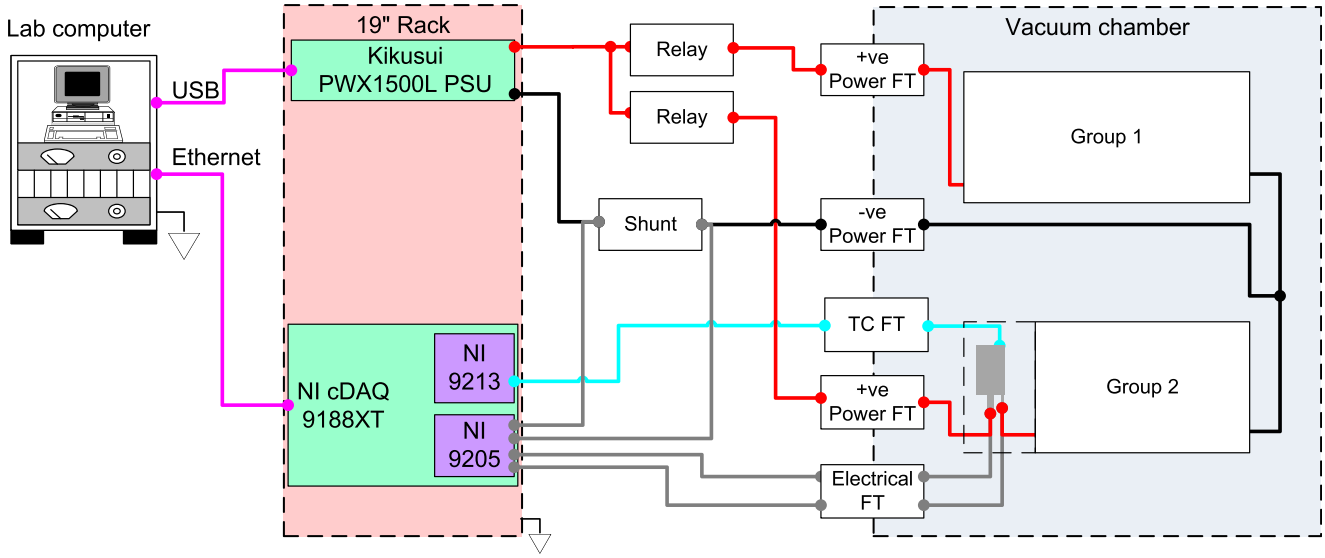

Fig. 3. Generic setup for STAR-BB-02 life testing (component- and assembly-level). A number of specimens are connected together in serial in 2 groups. The groups are wired in parallel, connected permanently to the ground terminal of the PSU (black), while relays alternately connect each group to the positive terminal (red). Voltage measurement leads connect to each specimen (grey), as well as to the shunt resistor. Type K thermocouples (blue) connect to the specimens.

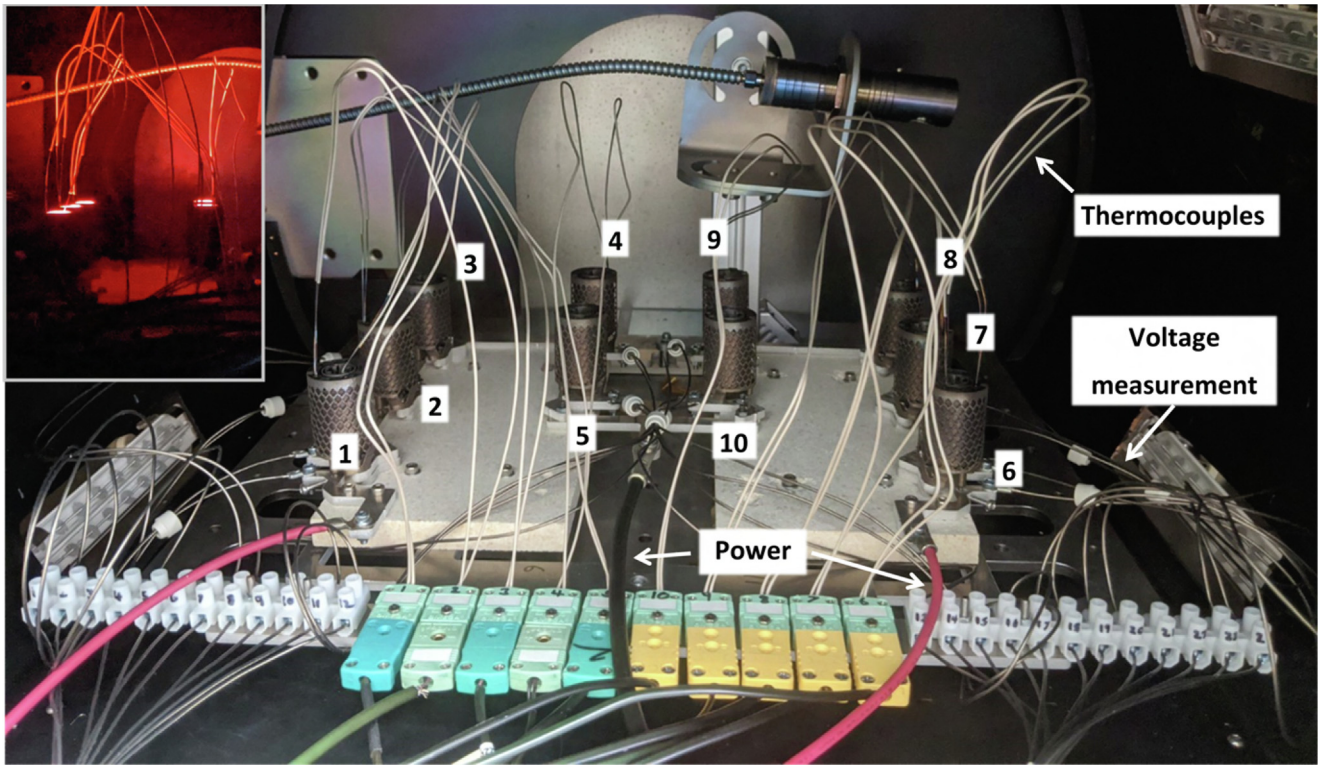

Fig. 5. Photograph of In625 component-level test setup inside hatch vacuum chamber. Thick red and black wires connect to the PSU, dark grey wires are for voltage measurement, and light grey wires are thermocouples. Heaters are numbered in correspondence with results section. Inset image shows heaters 1–5 during heating.

group of 2 Ta10W heaters. The specimens were heated for 5 min and cooled for 5 min in each cycle. The supply current was set to 30 A for Ta, and 28 A for Ta10W, corresponding to a target power of approximately 85 W at the beginning of the test. Thermocouples were attached to two Ta and two Ta10W heaters in position 2 as shown in Fig. 5. The third Ta heater was left uninstrumented, to provide a control case to indicate any effects of the thermocouples on the heater behaviour. Position 1 used for Inconel 625 was not populated in this test, as the predicted temperature of that location on the refractory heaters would exceed the temperature range of type K thermocouples. Following problems encountered in the In625 test, mineral-insulated thermocouples were used in place of bare junctions, to electrically isolate the thermocouple junctions from the heaters. The thermocouples were spot-welded in place. One Ta and one Ta10W heater also had a thermocouple in position 3. This was for the purpose of measuring the temperature experienced by the screws which would attach the heater into the thruster. These thermocouples were not included for In625 heaters as the temperature in this region is not high enough to be of concern.

Assembly-level tests were carried out as for the component-level tests, with a group of 5 thrusters fully constructed from In625 AM components, and a group of 3 which had pure Ta AM heaters and machined pure Ta nozzles. Due to limited facility availability, heating and cooling time were reduced to 2 min each per cycle to ensure sufficient cycling. This was chosen as an acceptable minimum time for representative testing, corresponding to a lower bound operational regime of 1 min of pre-heating and 1 min of thrusting. Based on the outcomes of the component-level tests, In625 thrusters were operated at 14 A, and Ta thrusters at 28 A. Each thruster was mechanically mounted inside the vacuum chamber, attached using ceramic standoffs for electrical and thermal isolation as in operation. A single mineral-insulated thermocouple was attached to the end of the case of each thruster near the nozzle exit, using Omegabond 600 high-temperature thermocouple cement. Fig. 6 shows the test setup. The test methodology did not include the use of propellant for every thruster in every cycle. The use of noble gas propellant means that there are no expected chemical interactions with the thruster material that would cause degradation. Pressure is also not expected to contribute to failure: the maximum intended operating pressure of the thruster is 10 bar, but only the outer casing experiences this full pressure differential. The pressure drop between each channel of the heater is negligible. Testing without propellant is conservative with respect to propellant at a given power as the peak temperature is higher. Each thruster is shown connected to a xenon gas supply, with one In625 thruster mounted horizontally on a thrust stand - it was initially intended to periodically supply propellant to each thruster, and measure thrust, flow rate and pressure at intervals during the life test to observe any changes. This was aborted as the thruster flow rates exceeded the pumping capacity of the vacuum chamber.

Table 2 tabulates the setting and measurement accuracy of the experimental setup. The independent variable was the power applied to the specimens, which was controlled by setting the regulated current of the PSU. The dependent variables were the heater's resistance and power, calculated from measured current and voltage, and the temperature. The current setting accuracy of the Kikusui PWX1500L PSU is 0.5% of the set current plus 0.1% of the current rating. The PSU current ripple noise is 300 mA RMS, or ±424 mA peak-peak assuming sinusoidal noise. The PSU load regulation is ±35 mA and line regulation is ±17 mA. This results in a total current setting accuracy of ±4.97% at a nominal current of 14 A, or ±2.75% at 28 A. Electrical measurements were carried out by the NI-9205 module. The module was operated in different ranges - the thruster voltage measurements were performed with a range of ±10 V, to accommodate all voltage inputs within the working range of the module. Taking the absolute accuracy at the full scale of 6.23 mV [11] as an upper bound, this yields an accuracy of

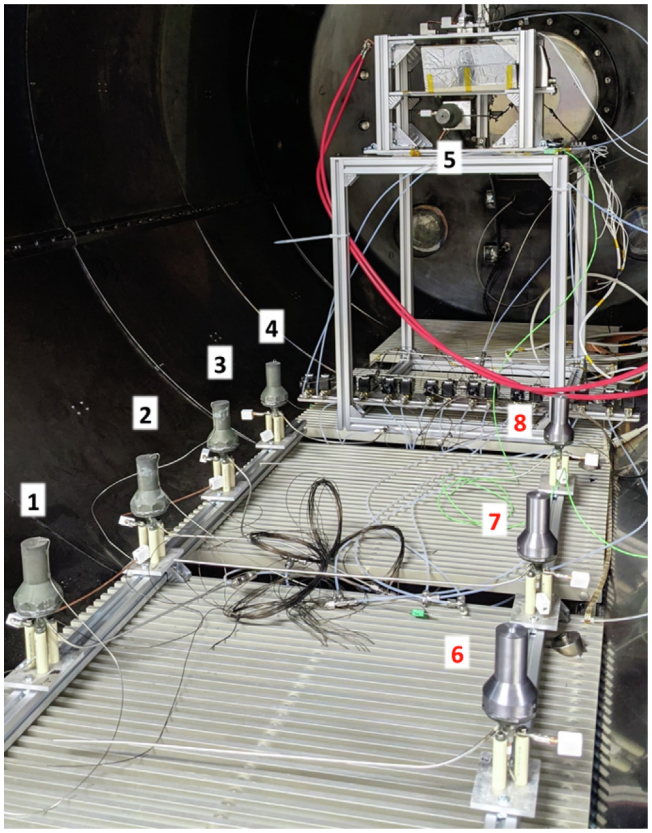

Fig. 6. Photograph of assembly-level test setup in main vacuum chamber. In625 thrusters are to the left of the image, with one mounted horizontally on the thrust stand frame at the rear, and are labelled in black. Ta thrusters appear to the right and are labelled in red. Thrusters are mounted on ceramic spacers for electrical and thermal isolation.

approximately 0.3% and 0.22% for voltage measurements on nickel alloy and refractory samples respectively. For the shunt resistor voltage measurement, the lowest input range of ±0.2 V was used, with absolute full-scale accuracy of 0.175 mV. The accuracy of the shunt resistor's electrical resistance is ±0.25%. The combined accuracy for current measurements, derived by adding the relative uncertainties of the shunt resistance and voltage measurement in quadrature [12], is therefore ±1.27% and 0.67% for 14 A and 28 A respectively. The accuracies for voltage and current are used with Eqn. 2 to calculate combined accuracies for electrical resistance and power of ±1.30% and ±0.71% for 14 A and 28 A. For temperature measurements, the NI-9213 module was operated in high-speed mode, giving an accuracy of 0.25 °C [13].

$$\frac{\Delta P}{P} \equiv \frac{\Delta R}{R} = \sqrt{\frac{\Delta I^2}{I} + \frac{\Delta V^2}{V}} \tag{2}$$

4.3. Test results

The test results of the component and assembly-level tests are presented separately in this section.

4.3.1. Nickel alloy component-level test results

All In625 heaters were powered at 14 A for cycles of 5 min heating and 5 min cooling. The test was terminated after a total of 6105 cycles. Fig. 7 shows the resistance behaviour for heaters 1 to 5 for the first 5 cycles, which are representative of the nominal behaviour of the heaters. The other 5 heaters behaved in the same way during these cycles so are omitted for clarity. Electrical resistance is plotted as an indicator of the heaters' behaviour because it is affected by the structure of the heater. For example, increasing resistance would indicate a reduction in cross-sectional area of some component of the heater, while a rapid decrease in resistance would indicate that the heater had deformed, leading to unintended physical contact between two parts. As the PSU was operated in constant current mode, heating power is directly proportional to the resistance, with the proportionality constant being the square of the current. During the cooling periods, no resistance is measured as the voltage across the heater is 0. During each cycle, the mean resistance is slightly over 150 mΩ, corresponding to approximately 30 W power. Table 3 shows the mean resistance value for each heater during the 1st cycle. The change in resistance during each cycle is negligible, with the standard deviation of resistance within each cycle shown being <1.5 mΩ, giving a relative standard deviation of approximately 1%. This constant value is explained by the low thermal coefficient of resistivity of In625 [15]. The resistance does not change significantly from one cycle to the next, with the mean in each subsequent cycle shown in Fig. 7 differing by significantly less than the standard deviation.

The resistance in the cycles shown is very repeatable between heaters. Comparing the mean resistance during the first cycle for each heater, the range between the maximum and minimum was 2.2 mΩ and the standard deviation was 0.8 mΩ. This indicates that the STAR-BB-02 heater design can be reliably manufactured in In625 via SLM - though as the heaters were produced in a single batch, further work would be needed to confirm that this is the case when production is scaled up, and different material batches

Table 2
Setting and measurement accuracy of instruments.

Item	Contribution	Stated value	Relative accuracy @ 14 A (%)	Relative accuracy @ 28 A (%)
Kikusui PWX1500L [14]	Setting accuracy	±0.5% setting ±0.5% full scale	1.57	1.04
	Ripple noise	300 mA RMS	3.03	1.52
	Load regulation	±35 mA	0.25	0.125
	Line regulation	±17 mA	0.121	0.061
Combined current setting accuracy			**4.97**	**2.75**
National Instruments NI-9205 [11]	Absolute accuracy at full range ±10 V	±6.23 mV	0.30	0.22
	Absolute accuracy at full range ±0.2 V	±0.175 mV	1.25	0.625
Murata 3020–01096-0	Resistance accuracy	±0.25%	n/a	n/a
Combined measurement accuracy of resistance or power			**1.30**	**0.71**
National Instruments NI-9213 [13]	Accuracy (high-speed mode)	±0.25 °C	n/a	n/a

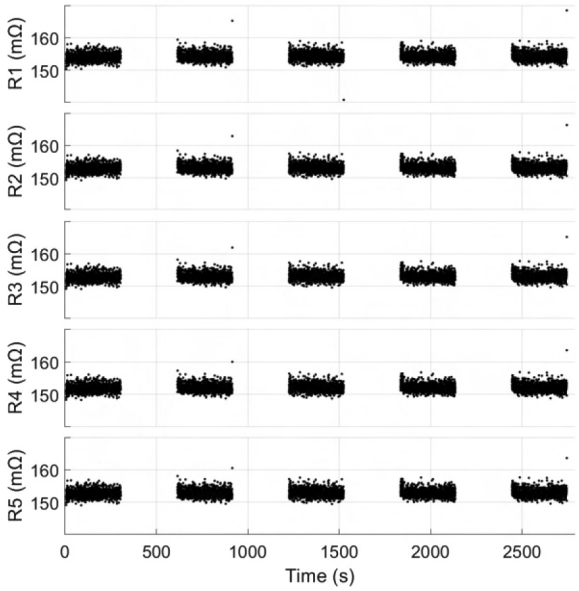

Fig. 7. Electrical resistance profile of In625 heaters 1 to 5 for first 5 cycles at 14 A. Each cycle consists of 300 s heating (resistance visible) and 300 s cooling, when resistance could not be measured.

Table 3
Mean resistance of each heater at 1, 2000, 4000 and 6000 cycles. Range (Δ) and standard deviation (σ) are calculated between the mean values for each heater. After cycle 1, heater 7 is excluded from the calculations. Excluded values are shaded.

#	$\overline{R}_1$ (mΩ)	$\overline{R}_{2000}$ (mΩ)	$\overline{R}_{4000}$ (mΩ)	$\overline{R}_{6000}$ (mΩ)
1	154.0	161.3	167.5	185.6
2	152.9	160.8	167.5	200.8
3	152.8	159.1	164.7	178.2
4	151.9	158.8	164.5	179.4
5	152.7	159.4	165.0	178.3
6	153.6	160.9	166.8	185.2
7	153.6	67.0	72.1	64.7
8	152.3	154.5	159.6	164.8
9	151.8	157.8	162.8	171.7
10	151.9	157.9	162.8	172.2
Δ	2.2	6.8	7.9	36.0
σ	0.8	2.1	2.6	10.3

and AM machines are used. An almost identical pattern of noise can be seen in each of the heaters shown in the figure - this is because the majority of the noise in the calculated resistance value derives from the current measurement, which was common to all heaters. High outliers can be seen at the end of cycles 2 and 5, and a low outlier on heater 1 at the end of cycle 3. These are due to slight timing differences in the measurement of the voltage and current, leading to a spurious resistance measurement at the moment of switch-off when both change rapidly.

Fig. 8 shows the resistance trend over all 6105 heating cycles for all 10 heaters. Red, green and blue points show the maximum, mean and minimum resistance respectively for a single cycle. The first 10 s (3.3%) of each cycle were omitted from the calculation, to remove the effects of switch-on transients. 7 of the 10 heaters show a stable resistance over all cycles, which increases gradually, first in an approximately linear fashion, accelerating after roughly 5000 cycles. Despite not initially having the highest resistance, heater 2 increased more rapidly than the others, and this heater failed to an open circuit on cycle 6045. Examination of the heater after the test found that the thin members at the centre, where the power density is the highest, and which hence reach

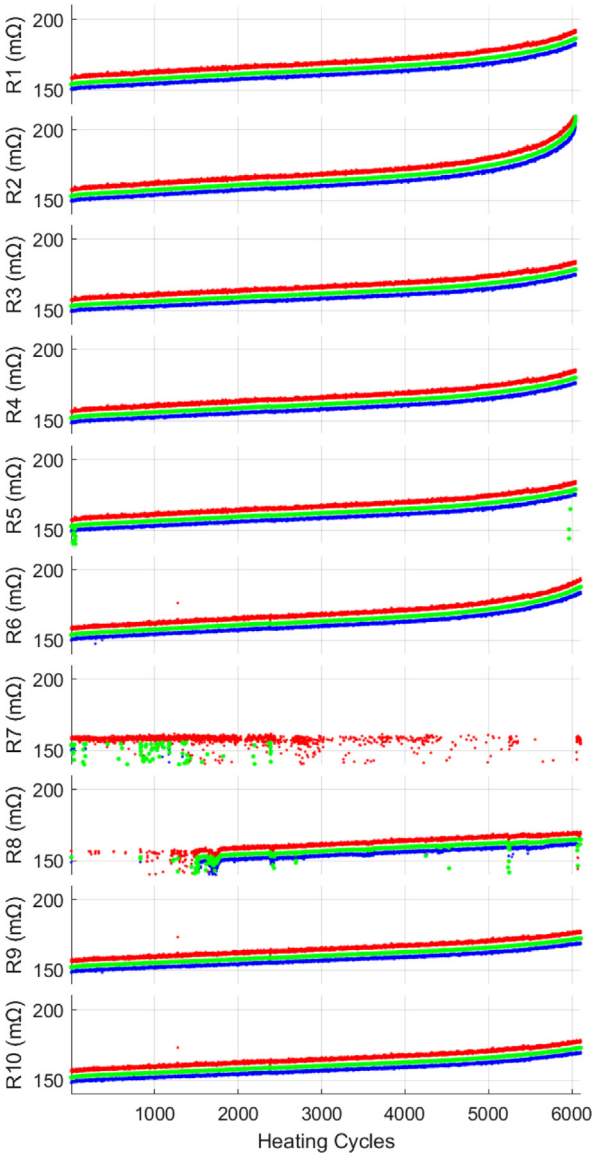

Fig. 8. Electrical resistance of all heaters for full test duration (6105 cycles). Each point represents one heating cycle, with red, green and blue representing maximum, mean and minimum resistance for the cycle, respectively.

the highest temperatures, had fractured. The fracture surfaces did not exhibit signs of melting or softening, which may indicate that the fracture occurred during cooling. This is similar to the failure mechanism encountered in the previous design iteration of the resistojet [16]. The accelerating increase of resistance indicates that the fracture was gradual. Due to the constant current operation of the power supply, any part of the heater which begins to neck due to thermal stresses has a higher resistance and hence locally increased heating, which increases the rate of damage by reducing the strength of the local material under the applied thermomechanical stress. In the cycles immediately before failure, the resistance and power of heater 2 reached 215 mΩ, 43% higher than in the 1st cycle. The constant current operation is a significant factor in this failure mode - operating at a constant voltage instead would reduce the local heating power in any necking region, which may act to hinder failure, though at the cost of reducing the heating power supplied to the thruster, possibly reducing its performance over time.

Heater 5 short-circuited during the first 70 cycles, as shown by a reduction in the minimum and mean resistance. This indicates that some part of the thruster deformed and touched another part, causing unwanted bypassing of the desired electric current path. After approximately 70 cycles, heater 5 recovered and behaved like the 7 nominal heaters. Heater 7 began to short-circuit within the first 100 cycles and did so for the remainder of the test. Heater 8 short-circuited consistently during the first 2000 cycles, whereafter it recovered and followed a similar trend to the other heaters, but occasionally short-circuited for the remainder of the test. A single increased maximum resistance point can be seen on heaters 6, 9 and 10 at approximately 1200 cycles - this is the result of a transient caused by the short-circuiting of heater 6, causing a spurious resistance reading.

Fig. 9 shows the 3 failed heaters with an expanded resistance scale, showing the short-circuiting behaviour more clearly. Note that the minimum resistance value is similar for all 3, in the range of 50–75 mΩ. Visual inspection of heater 8 after testing found that short-circuiting had occurred by bending of the coil at the centre of the heater, bringing it into contact with the surrounding cylinder. Heaters 7 and 8 also had slightly bent coils, but to a lesser extent. The tubes of heater 7 were not parallel, due to misalignment during assembly of the test rig - this is believed to be the reason why heater 7 became progressively worse, while heaters 5 and 8 recovered.

Temperature measurements from the bare junction thermocouples could not be taken while power was applied to the heaters, since the voltage interfered with the measurements. However, the thermocouples functioned properly in the 5-s period between cycles, when the PSU was turned off to allow the relays to switch. At the moment of switch-off, immediately after heating, the temperature of the two thermocouples in position 1 of heaters 1 and 6 was, respectively, 709 °C and 701 °C in the first cycle. These temperatures remained roughly constant for the test duration. A slow decrease to 5% below the initial value occurred until the 3000th cycle. This is believed to be caused by darkening and roughening (hence increasing emissivity) of the hot inner surfaces of the heaters, which was observed visually after the test. This resulted from

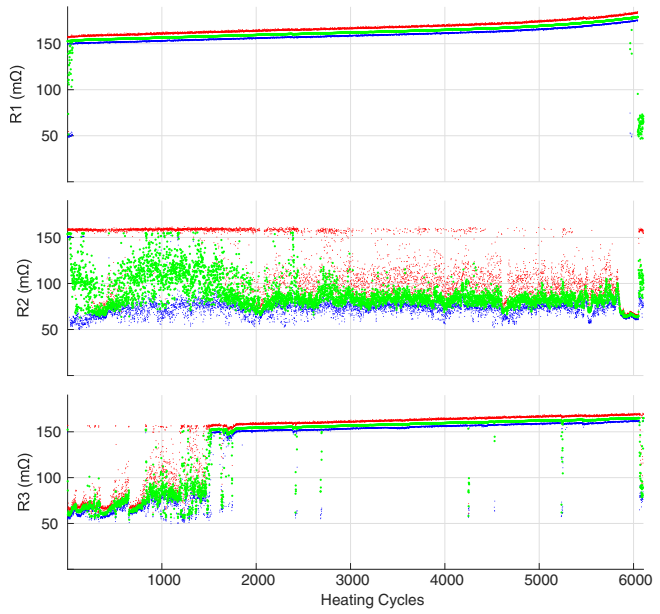

Fig. 9. Electrical resistance of 3 "failed" heaters for full test duration (6105 cycles). Each point represents one heating cycle, with red, green and blue representing maximum, mean and minimum resistance for the cycle, respectively. (Scott - the heater numbers are wrong in this. They will say 5, 7 and 8.).

reactions with material that outgassed from the plastic insulation of the thermocouple cables. In the latter half of the test, these temperatures gradually returned to approximately their initial values, due to increased heating power from the rising electrical resistance seen in Fig. 8. The temperatures recorded in position 2 for all 8 instrumented heaters were between 445 and 460 °C on the first cycle. Over the first 10–20 cycles this increased by approximately 10 °C for each heater, before plateauing. Thereafter, these temperatures gradually increased in proportion with the increasing resistance, with the exception of heaters 7 and 8 due to short-circuiting. At the end of each cooling cycle, all thermocouples of all heaters decreased to between 230 and 245 °C. This was less sensitive to the increasing resistance during the test. In the 5 s immediately after heating, the position 1 temperatures cooled by 50 °C while the position 2 temperatures cooled by only 2 °C. This trend is expected, as the hotter parts of the heater will have a higher radiative heat flux to the environment.

Following the fracture of heater 2, heaters 1, 3, 4 and 5 received no power due to the serial connection between them. Therefore the test was stopped shortly after the fracture. Heaters 7 and 8 are considered to have failed, despite the recovery of heater 8. The initial short-circuiting of 5 would not be acceptable in operation, but the heater recovered fully and rapidly after less than 2% of the test duration, and therefore can be counted as successful for the purposes of demonstrating heater endurance. Therefore, it can be concluded that 8 out of 10 heaters performed nominally for at least 6000 cycles. After 4000 cycles, the targeted minimum endurance, their electrical resistance had increased uniformly by approximately 9% compared to the first cycle. At that point, the relative range of resistance between the non-short-circuited heaters was 5%. These results show, for the first time, a high-temperature AM resistojet heater in flight candidate nickel alloy materials, exceeding the representative cycle life requirement at operational temperatures. Moreover, the similarity of behaviour from 10 heating elements indicates that the SLM manufacturing process is capable of producing repeatable components of this design.

4.3.2. Refractory component-level test results

3 pure Ta heaters were tested along with 2 made from Ta10W alloy. The heater design was the same as the In625 heaters, but the electrical terminals connecting to the test setup were altered to allow better alignment of the heater during assembly. Due to supply limitations of refractory parts, one of the Ta heaters (heater 3) used the old terminal design and was manufactured in a different batch to the other two. The Ta heaters were heated at 30 A, while the Ta10W heaters were heated at 28 A. This power was chosen from a previous test, to provide approximately equal power (nominal 85 W) to both materials, given the slightly higher resistance of the Ta10W heaters. The test was terminated after a total of 2560 cycles.

Fig. 10 shows the first 5 heating cycles of all heaters. The Ta10W heaters 1 and 2 are offset from the Ta heaters 3, 4 and 5 due to the alternate heating and cooling of the two sets. Compared to In625, the higher temperature coefficient of resistivity of tantalum [17] results in a slower and greater change in resistivity due to heating. The cold resistance of approximately 20 mΩ for each heater is 3–5 times lower than the hot resistance seen at the plateau of each cycle. Each cycle follows the same pattern of an initial rapid increase in resistance followed by a plateau, a trend seen in previous endurance tests of the STAR-0 prototype design using 316L stainless steel [16]. The refractory metal heaters had a greater variation in resistance between them than the In625 heaters. Both Ta10W heaters reached a similar resistance, with plateau values of 105 mΩ for heater 1 and 108 mΩ for heater 2. For pure Ta, heaters 4 and 5 reached 96 mΩ and 92 mΩ respectively, while heater 3 only reached 69 mΩ. This is not believed to be due to

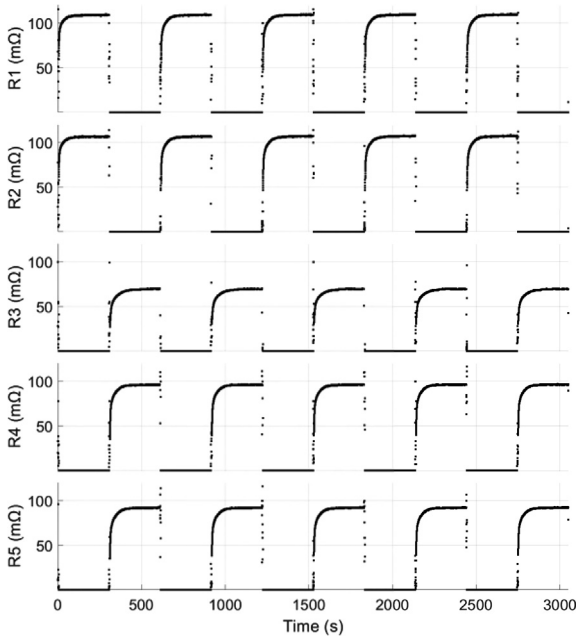

Fig. 10. Electrical resistance profile of refractory heaters for first 5 cycles at 28 A (Ta10W) and 30 A (pure Ta). Heaters 1 and 2 are Ta10W, heaters 3, 4 and 5 are pure Ta. Each cycle consists of 300 s heating (resistance visible) and 300 s cooling, when resistance could not be measured and so appears as 0.

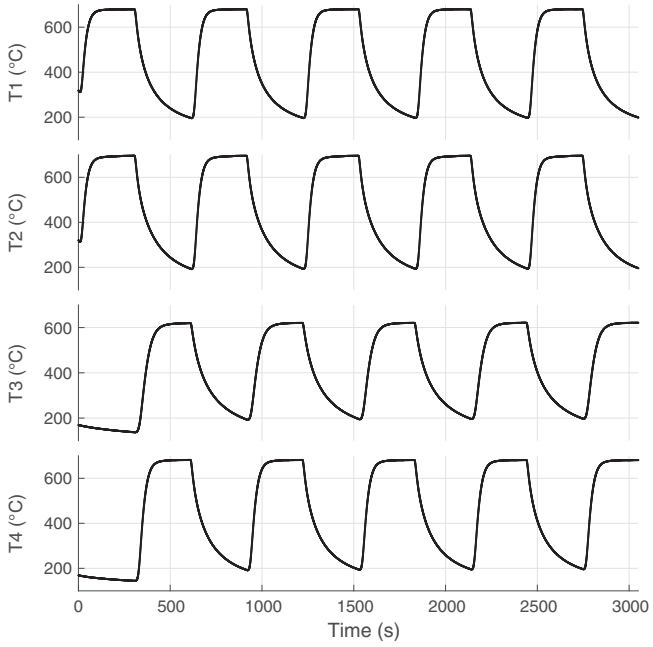

Fig. 11. Temperature of all refractory heaters for first 5 cycles at 28 A (Ta10W) and 30 A (pure Ta). Thermocouple number corresponds to heater number, heater 5 was uninstrumented. Each cycle consists of 300 s heating and 300 s cooling. Initial temperature is above ambient due to bake-out procedure before testing.

short-circuiting, due to the consistent profile shape which matches the other heaters. The variation may come from a range of factors: either heater 3 must have thicker walls, or the material must have lower resistivity or higher emissivity, or a combination of these. Each of these could arise as a result of differences in material batches or SLM processing parameters. Due to the strong coupling between temperature and resistance in Ta, a large discrepancy in hot resistance results from a relatively smaller difference in geometry or material properties. In production, refractory heater properties will have to be more tightly controlled than for nickel alloys, where there is no amplifying effect due to the lower temperature coefficient of resistivity. Due to the greater variability in resistance between the refractory heaters compared to In625, the power differed from the nominal value. The power of heaters 1–5 respectively in the first cycle was 85, 84, 63, 86 and 83 W. Despite the difference between heaters, each heater is repeatable between cycles.

Fig. 11 shows the thermocouple measurements in position 2 of the refractory heaters for the first 5 cycles. Heater 5 was not instrumented with thermocouples. Following the temperature measurement issue with the In625 heaters, mineral-insulated type K thermocouples were used instead of bare, grounded junctions, allowing continuous measurement during heating. The temperature profiles follow a similar pattern to electrical resistance, rapidly increasing before plateauing. This indicates that the heater rapidly reaches its operating temperature despite the initial low power, which is beneficial for operation. The thermocouple plateaus more slowly than the resistance, reaching 95% of the plateau value in under 2 min of heating. The faster plateauing of the resistance indicates that the central coil, which comprises the majority of the electrical resistance of the heater, reaches full temperature more quickly, while the remainder of the heater continues to heat up. Note that the initial temperature is above ambient, as a bakeout procedure was carried out on the heaters before the test to remove any moisture or other volatiles which might damage the oxidation-sensitive tantalum. The maximum temperature in position 2 was approximately 680 °C for heater 1, 695 °C for heater 2, 620 °C for heater 3 and 680 °C for heater 4. The lower temperature of heater 3 is attributed to the reduced resistance, hence reduced power. Since the main mechanism of heat loss from the high-temperature heater is thermal radiation, which is proportional to the 4th power of temperature, the relative reduction in temperature of heater 3 compared to the other heaters is less than the reduction in resistance.

Fig. 12 shows the resistance for all heaters during all 2560 cycles in the same format as Fig. 8. Only heater 5 demonstrated

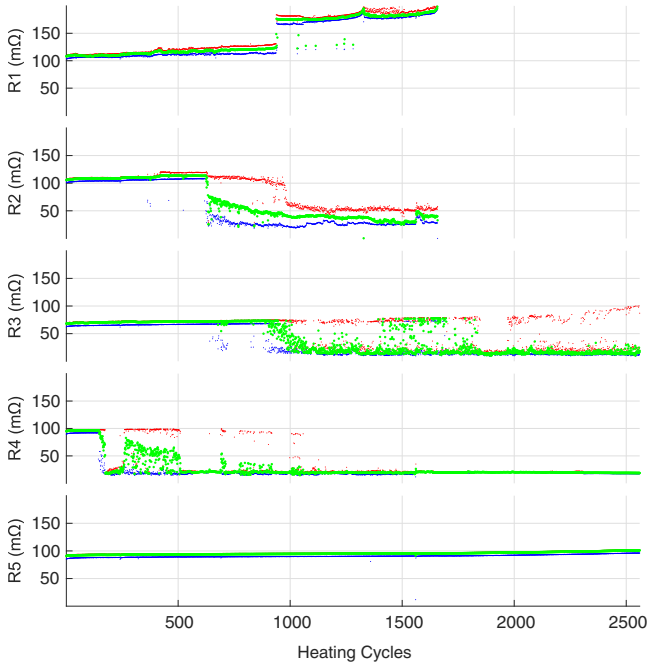

Fig. 12. Electrical resistance of all refractory heaters for full test duration (2560 cycles). Each point represents one heating cycle, with red, green and blue representing maximum, mean and minimum resistance for the cycle, respectively.

nominal cycling behaviour for the test duration. Fig. 13 shows the final 3 cycles of heater 5. Comparing this to the first 5 cycles, the plateau resistance is higher but the profile shape remains the same. Over the 2560 cycles, its mean resistance increased by 11%, from 89.9 mΩ to 100.9 mΩ. This is a greater rate of increase than was seen in the In625 heaters, which reached 11% increase after approximately 6000 cycles. Small dips in resistance are visible at approximately 240, 320, 690, 1360 and 1560 cycles - these are due to pauses in the test after which the heaters began cycling from a lower temperature. In these post-pause cycles, the minimum resistance (in the first seconds of heating) is lower, while the maximum and mean of the cycles are not significantly reduced - the plateau value was approximately the same.

The two other pure Ta heaters, heater 3 and heater 4, began short-circuiting after approximately 700 and 150 cycles respectively. The behaviour thereafter was similar to that seen in In625 heaters 7 and 8, with intermittent short-circuiting of increasing severity, resulting in a shift of the mean resistance from its nominal value to a consistent lower value, in this case near 20 mΩ. Of the Ta10W heaters, heater 2 failed by short-circuiting in the same way, after approximately 600 nominal cycles. Heater 1, meanwhile, failed to open circuit after 1650 cycles. Visual inspection after the test showed that the central coil had fractured in the same manner as In625 heater 2. Before this, a jump in the resistance of heater 1 occurred after approximately 900 cycles, from approximately 110 mΩ to 160 mΩ. The visual inspection showed that the outermost solid cylinder of the heater had a large azimuthal crack, shown in Fig. 14, as well as fractured areas of the outer mesh wall visible in the lower right of the image. It is hypothesised that this crack rapidly grew to cause the sudden increase in resistance. The crack is largely perpendicular to the AM build direction of the part. Heater 2 also had fractured areas of the outer mesh, which may account for the increase in its resistance at around 300–500 cycles, but it did not have such a crack in the solid wall. No such cracks were found in the pure Ta or In625 heaters; this indicates that the cracks are more likely a consequence of the material than of the design. Ta10W has lower ductility than pure Ta due to the addition of W. However, it is commonly used in high-temperature applications, including in wire form in heating elements, suggesting that the alloy is not, per se, inadequate for the present application. This suggests that the AM process may be the root cause of the cracking. A dedicated AM parameter set was not developed for Ta10W in this project - parameters for pure Ta were used instead. Ta10W has a slightly higher melting point and thermal conductivity than that of pure Ta. All else being equal, a laser energy density suitable for pure Ta may therefore be insufficient to achieve full melting of each layer in Ta10W. Inadequate bonding between layers due to undermelting would explain the orientation of the cracks parallel to the layers. In addition to this, W is widely reported to be prone to microcracking during AM processing (e.g.[18]), which is not the case for Ta. This may be a factor in the observed material failure. While speculative, these observations indicate that development of an optimised AM parameter set may be fruitful for use of Ta10W in future.

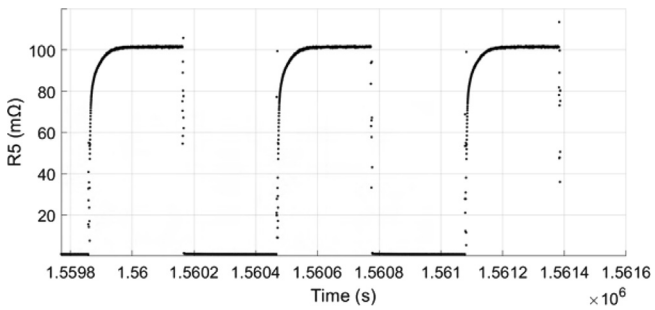

Fig. 13. Electrical resistance profile of pure Ta heater 5 for final 3 out of 2560 cycles at 30 A.

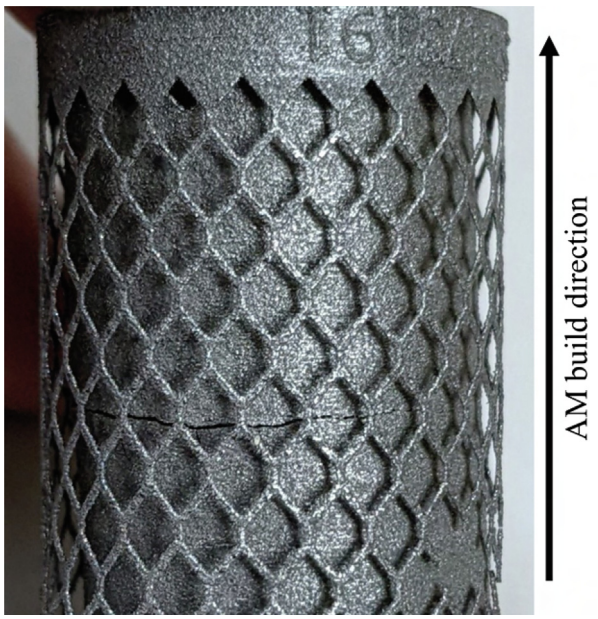

Fig. 14. Azimuthal crack and fractured mesh found on visual inspection of Ta10W heater 1 following life test.

Due to the failures of 4 of the 5 heaters, this test was terminated early after 2560 cycles to allocate more time to the assembly-level testing. There was greater variability between refractory heaters than In625 heaters, though the sample size was smaller. Despite the use of a new mechanical interface intended to provide better alignment during assembly, 3 out of 5 refractory heaters short-circuited. On visual inspection after testing, the central coil of the refractory heaters was more significantly distorted than that of the In625 heaters. A single pure Ta heater, heater 5, exhibited nominal behaviour for the entire test duration, constituting over 60% of the target duration. Over this time, the relative increase in resistance from the beginning of the test was larger than that seen in In625.

4.3.3. EM thruster assembly-level test results

In625 thrusters were operated at 14 A to achieve the same 30 W power used in the component life tests. Ta thrusters were operated at a lower current of 28 A to test at a lower power of 60 W compared to the 85 W of the component-level test, due to the high rate of increase of resistance seen in Ta heater 5 compared to the In625 heaters. The assembly-level test was run for a total of 10237 cycles.

Fig. 15 shows the resistance of 5 of the 8 EM thrusters for the full test duration of 10237 cycles, in the same format as Fig. 8. Thrusters 1–2 are In625 and thrusters 6–8 are Ta. Following the high proportion of refractory heaters which short-circuited, a ceramic insulator ring component which sits at the open end of the heating element (see Fig. 2) was modified to interlock with the heater channels, holding the cylinders concentric and preventing rotation between them. This was initially only fitted to the Ta thruster assemblies, as the distortion of the In625 heaters had been less severe - the modification replaces a simple axisymmetric ceramic component with a complex geometry that requires multi-axis machining. However, early in the assembly-level life test, all In625 thrusters began to short-circuit, while Ta heaters did not. The 3 In625 thrusters omitted from Fig. 15 behaved similarly to thrusters

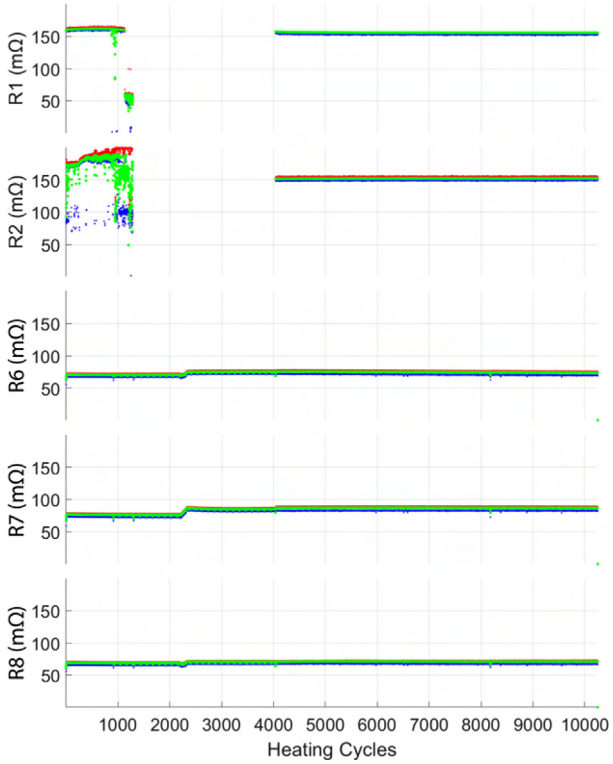

Fig. 15. Electrical resistance of 5 EM thrusters for full test duration (10237 cycles). Each point represents one heating cycle, with red, green and blue representing maximum, mean and minimum resistance for the cycle, respectively. Thrusters 1–2 are In625, thrusters 6–8 are Ta.

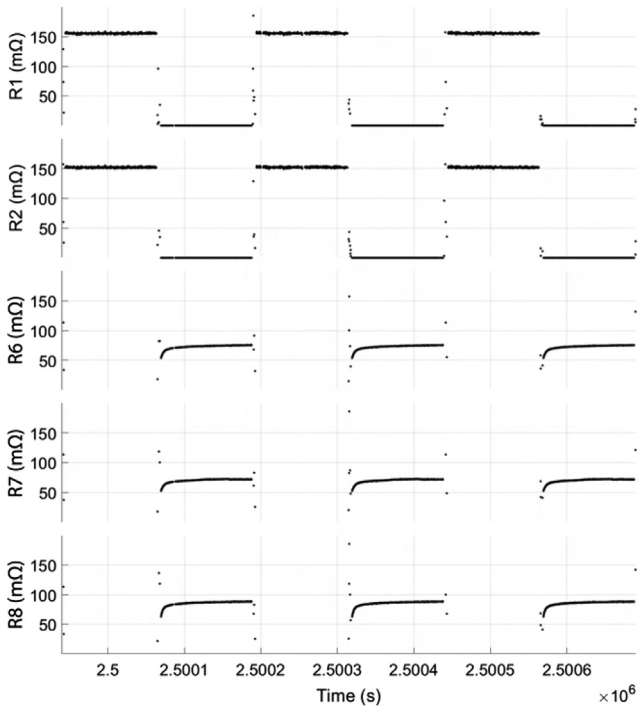

Fig. 16. Electrical resistance profile of EM thrusters for cycles 10000–10002.

1 and 2. It was inferred that the In625 heaters' central coils were distorting sufficiently to touch the nozzle, which is positioned in the centre of the heater, reducing the physical margin before contact compared to the bare heater. Additional modified ceramic rings were procured, but only 2 could be obtained in the testing period. These were retrofitted into In625 thrusters 1 and 2 after the Ta thrusters had completed 4000 cycles. In the meantime, the In625 thrusters were switched off.

Following the installation of the new ceramic rings, the short-circuiting was eliminated and did not re-occur for the remainder of the test. In625 thrusters 1 and 2 achieved nominal cycling behaviour for 6000 cycles thereafter. Fig. 16 shows the resistance of the 2 functioning In625 and 3 Ta thrusters in the 3 final cycles of the test (after 6000 In625 cycles and 10000 Ta cycles), showing that the In625 thrusters have a flat resistance profile as was seen in the component tests. The resistance at the beginning of the component- and thruster-level tests is very similar, with thruster 1 and 2 having a mean resistance of 157.4 and 151.5 mΩ respectively on their first cycle. After the 6000th cycle, thruster 1 had reduced to 155.6 mΩ. This is believed to be due to internal resistance of the connection between the heater and its power connection reducing over time. Thruster 2 increased by 0.4% to 152.1 mΩ, much less than the increase seen in the bare heaters over the same duration at the same power. This may indicate that the presence of the nozzle either reduces the peak temperature in the heater, or changes the temperature distribution in a way which reduces the rate of degradation.

The tantalum heaters achieved 10000 cycles of normal operation with no short-circuiting. At the start of the test, the mean resistance in each cycle was 70.9, 76.8, and 69.0 mΩ for thrusters 6, 7 and 8 respectively. Fig. 16 shows that the resistance profile is similar to that of the bare refractory heaters, with an initial rapid increase in resistance followed by a plateau. The plateau resistance is lower than that in the bare heater tests, indicating a lower peak temperature due to the lower input power. As with the bare heater testing, a number of brief dips in the minimum resistance can be seen, due to pauses in testing. Periodic smaller dips can be seen between 800 and 4000 cycles. These were caused by xenon gas which was fed to the thrusters in this period, cooling the heaters. This aspect of testing was aborted because the resistojet flow rate exceeded the pumping capacity of the testing facility, which is primarily intended for testing ion thrusters. A jump in resistance of all 3 Ta thrusters is seen at approximately 2200 cycles. This is believed to be due to volatiles being released into the test chamber as xenon saturated the chamber's cryopanels. Tantalum is extremely prone to oxidation at high temperatures. The thrusters continued to operate nominally after this event, at a slightly increased resistance. The resistance at the end of testing was 73.7, 86.8 and 70.8 mΩ respectively, an increase of 4, 13 and 3 % compared to the beginning of the test. Most of this came from the common increase at 2200 cycles. Thruster 7, which had both the greatest increase at that time, and the highest overall resistance, operated at a power of 68 W for 7000 cycles. This is cause for cautious optimism that higher power operation is sustainable for Ta without significant degradation. However, further work is needed to confirm this. In particular, uncertainty as to the cause of the jump in resistance means that it cannot be guaranteed that the additional 8 W of heating power in thruster 7 were distributed through the heater in the same way that would be achieved by increasing the current.

5. Materials properties and failure discussion

The experiments described here show that AM heat exchangers can operate at high temperatures for more than 4000 cycles. However due to the complexity of the design, measurements of the temperature in the hottest parts of the thruster were not possible, and it is therefore of interest to consider the material properties and possible failure modes found in the thrusters. At very high

temperatures, multiple failure modes are possible. Examination of any persistent changes in the material is beyond the scope of this paper, so it is assumed for this analysis that the properties did not change from one cycle to the next. However, raising a metal to very high temperatures lowers its strength and stiffness, which can result in creep. Due to the cyclic nature of operation, fatigue failure may also occur.

In the component level tests, 2 In625 heaters and 1 Ta10W heater failed to an open circuit. In all cases this failure was seen at the same point in the middle of the heater's central coil. The approximate location is indicated in Fig. 17. The same failure location was also observed in a preliminary test, where a single In625 heater was (non-cyclically) heated with progressively higher currents until it melted. That failure indicated that the middle of the coil reaches the highest temperature in the thruster, hence melting before any other part in the preliminary test. As such, it can be expected that the strength of the material, whether refractory or nickel alloy, will be lowest at this location. However, by design, this part of the coil should also experience low thermomechanical stress, as it is able to expand and contract with little constraint.

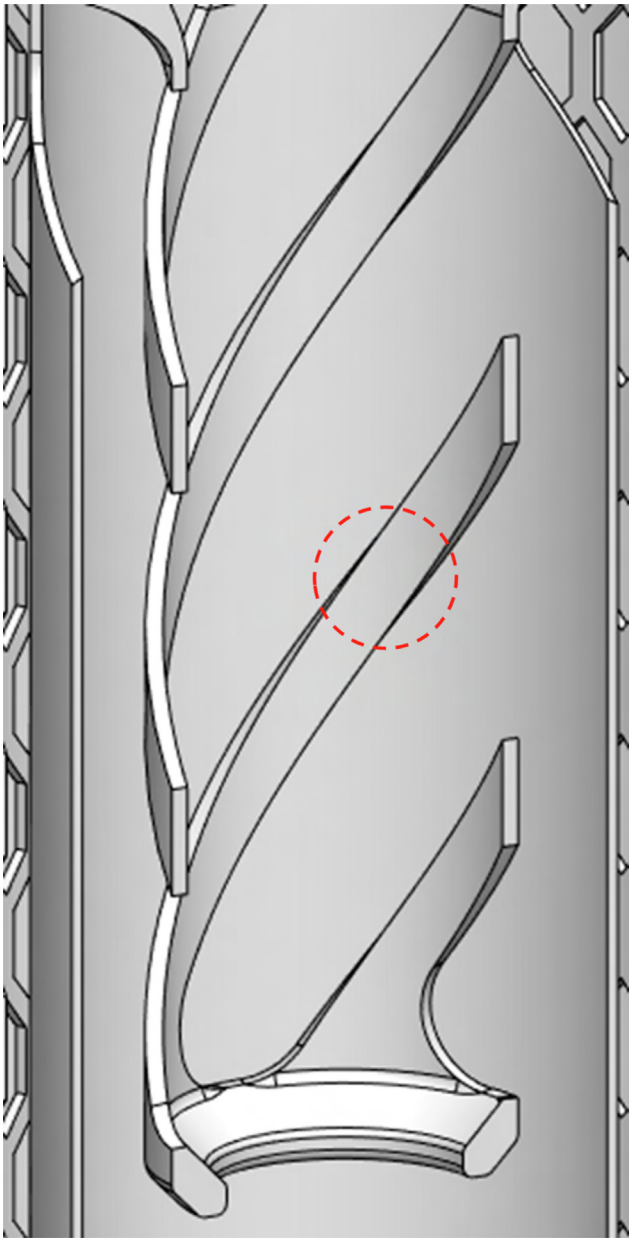

Fig. 17. Sectioned CAD image of coil structure at the centre of the heater. The red circle indicates the approximate location of all observed open-circuit failures.

Multiphysics simulations were carried out in COMSOL on the full 3D geometry of the thruster. There is little experimental data to validate these simulations in the most important region of the coil, as this location could not be instrumented with thermocouples. However, at multiple electric powers, the highest temperature in the simulations was consistently found in the approximate location where the failures were observed, while the highest thermomechanical stress was found at the root of the coil, where it connects to the concentric cylinders of the heater. The coil is designed to have a higher heating power density than the cylinders. Therefore there is a large temperature gradient between the coil and the cylinders, which is why the stress at the interface between them is higher than in either the cylinders or the coil themselves. Therefore the simulations suggest that the observed failure location is at the highest temperature, but not at the location of highest stress. Simulations of In625 at 30 W indicate that the maximum stress over a 300 s heating period reaches 166 MPa at the coil root. Meanwhile, the simulated temperature at that location did not exceed 900 K. At this temperature, the yield stress of In625 (manufactured either by forging [19] or by SLM [20]) is approximately 4–500 MPa, significantly higher than the predicted stress allowing for uncertainty in the simulation. The maximum simulated stress at the failure point was 45 MPa, at a simulated temperature of 1300 K. At approximately this temperature, the yield strength is around 100 MPa. However, at this elevated temperature the yield strength is much more sensitive to temperature than at 900 K. Therefore it is possible, given the lack of validation of the simulations to date, that the actual stress at the failure point could be higher than the yield strength. Given this, it should be expected that some combination of creep and/or low-cycle fatigue damage may be the cause of the observed cyclic failures. In addition to this, simulations including xenon flow at representative pressures planned for operation (1–4 bar and 50–200 MPa) indicate that the maximum temperature and stress are slightly lower than in the dry case. This indicates that the dry tests presented here are conservative with respect to operation.

There is little literature surrounding very high temperature properties of In625. Several peer-reviewed publications indicate cycle lives in excess of 10000 at temperatures between 973 and 1073 K for conventionally manufactured samples [21–23], and Ghiaasiaan et al. [24] found that In625 produced by SLM had a cycle life over 10000 at 922 K. No data could be found at or above 1400 K, however three publications discuss properties at 1373 K. Ghoussoub et al. [20] investigated the tensile properties of In625 produced by SLM, finding a yield strength of approximately 100 MPa at 1373 K. Purohit et al. [25,26] disclosed fatigue tests on cast samples at this temperature, finding a maximum life of 6000 cycles for specimens tested at an applied strain of 0.4 % in reversed bending and over 10000 at axial push–pull strain ranges below 0.15 %. They further remark that creep damage was a significant factor at 1373 K. While this literature is sparse, it does indicate that cyclic operation of In625 has been achieved at relevant temperatures and cycle life for STAR to meet its target performance. These results were achieved at low load conditions, however the STAR heater has been designed to reduce thermomechanical stresses in the hottest regions.

No relevant literature could be found for the fatigue properties of Ta or Ta10W at very high temperatures. However, Ta10W is expected to be less ductile than Ta due to the addition of W. The Ta10W heaters in the component-level test were found to have not only failed in the coil, but also to have large cracks in the outer cylinders. Given the relatively low temperatures in this location, it is likely that these failures represent some underlying defect in the SLM process for this material. Ta10W itself is a commonly used

alloy for high-temperature fasteners and wire, and therefore there is no reason to suspect that the base alloy is unsuitable for this application. However, in the present work it was manufactured without optimised SLM parameters.

6. Conclusions

This paper has presented the results of cyclic endurance tests on a novel high-temperature additive-manufactured resistojet, at the component level and on engineering-model thruster assemblies. The targeted minimum endurance was 4000 cycles, considered to envelope the number of heating cycles necessary for the primary propulsion system of a small LEO satellite. This target was exceeded by thruster assemblies with heaters made from Inconel 625 nickel superalloy, and from tantalum.

In initial component-level tests, seven out of ten In625 heaters operated nominally for over 6000 cycles at an initial power of 30 W. The test was terminated after the failure of one heater to an open circuit at 6045, due to fracture of the central coil. The remaining three heaters incurred short-circuiting failures of varying severity: one recovered completely and completed over 6000 nominal cycles, one partially recovered and completed 4000 cycles with intermittent short-circuiting, and one short-circuited for the entire test duration. In a component-level test of three pure tantalum and two tantalum-10% tungsten alloy heaters, one of the Ta heaters survived for over 2000 cycles, with an initial power of approximately 83 W. The test was ended due to the failure of 4 out of the 5 heaters: two Ta heaters short-circuited, along with one of the Ta10W heaters. The other Ta10W heater had fractures in its cylindrical walls, and failed to an open circuit due to eventual fracture of the coil, in the same way as the In625 heater. The testing of multiple heaters in parallel demonstrated the ability to consistently manufacture In625 heaters, with very little variability in electrical and thermal characteristics.

In assembly-level tests, a ceramic component was modified to prevent the short-circuiting failures seen in component-level tests. Three Ta thrusters, equipped with this component from the outset, completed over 10000 cycles. Due to resistance variation between the three thrusters, their initial operating power was 53–60 W. After 2200 cycles, due to an increase in resistance attributed to a facility fault, the thruster power increased to 55–68 W. There was no apparent adverse effect observed from operation at elevated power for 7800 cycles. Two In625 thruster, retrofitted with the modified ceramic partway through the test, completed over 6000 cycles at 30 W input power. The resistance increase over the duration of the thruster tests was negligible, despite operating at the same power as the component-level tests. This indicates that the thermal stress cycling is less extreme in the thrusters compared to the bare heaters. This may be due to some combination of slower cooling of the heater coil in the thruster assembly reducing thermal shock, lower peak temperature due to the heat sink of the nozzle, or altered temperature (hence stress) distribution. In any case, this indicates that, for a given operating power, the component-level tests were conservative with respect to testing at the assembly level.

The open-circuit failures seen in the In625 and Ta10W component-level tests were fractures of the heaters' central coils, occurring in the same location for both materials. This indicates a similar failure mechanism despite the very different materials and temperatures (approximately 1300K for In625 and 2000K for Ta10W). Operation of the heaters in the constant current mode used throughout is the worst case for this failure mode: as part of the heater necks or begins to fracture under thermomechanical loads, local heat generation increases, heating and softening the area further. From a spacecraft perspective, the resulting increased power draw if the heater is operated in constant current mode may also be problematic. Operation at constant power would be better in this regard, ensuring predictable power draw from the spacecraft. As the relative power density in the necking region increases compared to the rest of the heater, a constant power condition would still lead to increased local heating, but at a lower rate than constant current. A constant voltage condition would be the most benign from the perspective of this failure mode, resulting in reduced local heating. The disadvantage of this would be reduced total heating power to the thruster - however, if the rate of degradation is reduced significantly by the constant voltage, this may not be an issue. Further work is required to assess the effects of different operating modes on the thruster lifetime.

The success of the modified ceramic ring in preventing short-circuiting in assembly-level tests indicates that the BB-02 design heaters require careful alignment to achieve reliable operation. Therefore careful attention will be needed in future designs to facilitate this or improve the robustness of the heater to deformation.

This work has demonstrated for the first time that engineering-model high-temperature resistojets, additive-manufactured from flight candidate materials Inconel 625 and tantalum, can exceed endurance requirements representative of primary propulsion applications on small LEO spacecraft. The work has shown a lower bound endurance of 6000 cycles for In625 at a lower bound power of 30 W, and a lower bound endurance of 10000 cycles for Ta at a lower bound power of 60 W. Qualitatively similar trends between tests indicate that thrusters of this design can probably be operated at increased powers while still meeting the endurance target of 4000 cycles. However, further work is necessary to better characterise the relationship between power and endurance. Separate work by the author (in a publication to follow) shows that at 30 W, the power tested here, an In625 thruster can produce 56.2±0.6 s I_{sp}. The present work therefore demonstrates that reliable operation of an AM resistojet in In625 is possible at 15 % greater I_{sp} than the commercial state of the art. This is a crucial step in confirming the operational feasibility of an AM high-performance resistojet.

7. Data availability

The raw/processed data required to reproduce these findings cannot be shared at this time due to technical or time limitations.

Declaration of Competing Interest

The authors declare that they have no known competing financial interests or personal relationships that could have appeared to influence the work reported in this paper.

Acknowledgements

The work in this paper forms part of a PhD studentship funded through the Centre for Doctoral Training in Sustainable Infrastructure Systems (CDT-SIS) at University Of Southampton. The funding is provided by the UK Engineering and Physical Sciences Research Council (EPSRC) under Grant No. EP/L01582X/1. Additional funding was provided by the UK Space Agency as part of both the RADICAL project, and the STAR (Super High Temperature Resistojets for All-Electric Telecommunication Satellites) Flagship grant, as well as the National Space Technology Program 2 via Innovate UK. The authors would like to thank Kevin Smith, Simon Beever and David Thurley at the University's EDMC workshop for their assistance in manufacturing. The authors also thank David Gibbon at Surrey Satellite Technology Ltd., Charlie Birkett and Cameron Breheny at HiEta Technologies Ltd., and Paul Aimone at H.C. Starck Inc. for their contributions as part of the STAR Flagship consortium.

The authors give thanks especially to Dr. Angelo Grubišić. Dr. Grubišić passed away in August 2019 before seeing the outcome of this work, which he originated. In addition to securing the funding that made the work possible, he was instrumental in supporting the authors in his capacity as supervisor, mentor and friend.

References

[1] BryceTech. Smallsats by the numbers 2021. Technical report, BryceTech, 2021. URL https://brycetech.com/reports/report-documents/Bryce_Smallsats_2021.pdf. Accessed on 10/01/2022.

[2] D. Nicolini, D. Robertson, E. Chesta, G. Saccoccia, D. Gibbon, A. Baker, Xenon resistojets as secondary propulsoin on ep spacecrafts and performance results of resistojets using xenon, in: Proceedings of 28th International Electric Propulsion Conference, Toulouse, France, 2003.

[3] D. Lev, G.D. Emsellem, A.K. Hallock, The rise of the electric age for satellite propulsion, New Space 5 (1) (2017) 4–14, https://doi.org/10.1089/space.2016.0020.

[4] V. Garcia, Ep system development and functional validation tests for the electra geo satellite, in: Proceedings of 36th International Electric Propulsion Conference, Vienna, Austria, 2019. URL https://electricrocket.org/2019/288.pdf.

[5] M. Leomanni, A. Garulli, A. Giannitrapani, F. Scortecci, Precise attitude control of all-electric geo spacecraft using xenon microthrusters, in: Proceedings of 33rd International Electric Propulsion Conference, Washington D.C., USA, 2013. URL https://electricrocket.org/IEPC/fhag9gda.pdf.

[6] J. Jack and E. Spisz. Nasa research on resistance-heated hydrogen jets. In Electric Propulsion Conference, page 1, 1963. doi: 10.2514/6.1963-23. https://arc.aiaa.org/doi/abs/10.2514/6.1963-23.

[7] F. Romei, A.N. Grubišić, Validation of an additively manufactured resistojet through experimental and computational analysis, Acta Astronaut. 167 (2020) 14–22, https://doi.org/10.1016/j.actaastro.2019.10.046. ISSN 0094–5765. URL http://www.sciencedirect.com/science/article/pii/S0094576519313748.

[8] F. Romei, High-Temperature Resistojets for All-Electric Spacecraft PhD thesis, University of Southampton, 5 2019.

[9] M. Robinson, A.N. Grubišić, G. Rempelos, F. Romei, C. Ogunlesi, S. Ahmed, Endurance testing of the additively manufactured star resistojet, Materials & Design 180 (2019) 107907, https://doi.org/10.1016/j.matdes.2019.107907. ISSN 0264–1275. http://www.sciencedirect.com/science/article/pii/S0264127519303454.

[10] F. Romei and M. Robinson. Electric heating system for heating a fluid flow. https://patentscope.wipo.int/search/en/detail.jsf?docId=WO2022111968, 2022.

[11] National Instruments Corporation. Ni 9205 datasheet. Technical report, National Instruments Corporation, 2017. URL https://www.ni.com/pdf/manuals/378020a_02.pdf. Accessed on 11/01/2022.

[12] J.H. Williams. Guide to the expression of uncertainty in measurement (the gum). In Quantifying Measurement, 2053–2571, pages 6–1 to 6–9. Morgan and Claypool Publishers, 2016. ISBN 978-1-6817-4433-9. doi: 10.1088/978-1-6817-4433-9ch6. doi: 10.1088/978-1-6817-4433-9ch6.

[13] National Instruments Corporation. Ni 9213 datasheet. Technical report, National Instruments Corporation, 2016. URL https://www.ni.com/pdf/manuals/374916a_02.pdf. Accessed on 11/01/2022.

[14] Kikusui. Pwx series user's manual. Technical report, Kikusui, 2021. URL https://manual.kikusui.co.jp/P/PWX_V6_E7.pdf.

[15] E. Kaschnitz, L. Kaschnitz, S. Heugenhauser, Electrical resistivity measured by millisecond pulse heating in comparison with thermal conductivity of the superalloy inconel 625 at elevated temperature, Int. J. Thermophys. 40 (3) (2019) 27, https://doi.org/10.1007/s10765-019-2490-8. Feb. ISSN 1572–9567. 10.1007/s10765-019-2490-8.

[16] M. Robinson, A.N. Grubišić, G. Rempelos, F. Romei, C. Ogunlesi, S. Ahmed, Endurance testing of the additively manufactured star resistojet Materials & Design 180 (2019) 107907, https://doi.org/10.1016/j.matdes.2019.107907. ISSN 0264–1275. https://www.sciencedirect.com/science/article/pii/S0264127519303454.

[17] N.D. Milošević, G.S. Vuković, D.Z. Pavičić, K.D. Maglić, Thermal properties of tantalum between 300 and 2300 K, Int. J. Thermophys. 20 (4) (1999) 1129–1136. July.

[18] B. Vrancken, R.K. Ganeriwala, A.A. Martin, M.J. Matthews, Microcrack mitigation during laser scanning of tungsten via preheating and alloying strategies, Additive Manufacturing 46 (2021) 102158, https://doi.org/10.1016/j.addma.2021.102158. ISSN 2214-8604. URL https://www.sciencedirect.com/science/article/pii/S2214860421003225.

[19] M.M. de Oliveira, A.A. Couto, G.F.C. Almeida, D.A.P. Reis, N.B. de Lima, R. Baldan, Mechanical behavior of inconel 625 at elevated temperatures, Metals 9 (3) (2019), https://doi.org/10.3390/met9030301. ISSN 2075–4701. https://www.mdpi.com/2075-4701/9/3/301.

[20] J. Ghoussoub, T. Tang, W. Dick-Cleland, A. Németh, Y. Gong, D. Mccartney, A. Cocks, R. Reed, On the influence of alloy composition on the additive manufacturability of ni-based superalloys, Metallurgical and Materials Transactions A 53 (2022) 01, https://doi.org/10.1007/s11661-021-06568-z.

[21] M. Bashir, R. Kannan, R. Sandhya, and G.A. Harmain. Low cyclic fatigue behavior of alloy 625 at ambient and elevated temperatures. In Raghu V. Prakash, R. Suresh Kumar, A. Nagesha, G. Sasikala, and A.K. Bhaduri, editors, Structural Integrity Assessment, pages 653–661, Singapore, 2020. Springer Singapore. ISBN 978-981-13-8767-8.

[22] L. Mataveli Suave, J. Cormier, D. Bertheau, P. Villechaise, A. Soula, Z. Hervier, F. Hamon, High temperature low cycle fatigue properties of alloy 625, Materials Science and Engineering: A 650 (2016) 161–170, https://doi.org/10.1016/j.msea.2015.10.023. ISSN 0921–5093. https://www.sciencedirect.com/science/article/pii/S092150931530486X.

[23] Z. Wu, X. Chen, Z. Fan, Y. Zhou, J. Dong, Studies of high-temperature fatigue behavior and mechanism for nickel-based superalloy inconel 625, Metals 12 (5) (2022), https://doi.org/10.3390/met12050755. ISSN 2075–4701. https://www.mdpi.com/2075-4701/12/5/755.

[24] R. Ghiaasiaan, A. Poudel, N. Ahmad, P.R. Gradl, S. Shao, and N. Shamsaei. High temperature tensile and fatigue behaviors of additively manufactured in625 and in718. Procedia Structural Integrity, 38:581–587, 2022. ISSN 2452–3216. doi: 10.1016/j.prostr.2022.03.059. https://www.sciencedirect.com/science/article/pii/S2452321622002724. Fatigue Design 2021, International Conference Proceedings, 9th Edition.

[25] A. Purohit, U. Thiele, and J.E. O'Donnell. Fatigue strength and evaluation of creep damage during fatigue cycling of inconel alloy 625. Proceedings of American Nuclear Society winter meeting, San Francisco, CA, USA, 6 1983a. https://www.osti.gov/biblio/5906535.

[26] A. Purohit, I.G. Greenfield, and K.B. Park. High-temperature reverse-bend fatigue strength of inconel alloy 625. Proceedings of American Nuclear Society winter meeting, San Francisco, CA, USA, 6 1983b. https://www.osti.gov/biblio/5864115.